Extreme Mechanics Letters 9 (2016) 66–73

Contents lists available at ScienceDirect

Extreme Mechanics Letters

journal homepage: www.elsevier.com/locate/eml

Large deformation effect in Mode I crack opening displacement of an Agar gel: A comparison of experiment and theory

Rong Long [a], Maxime Lefranc [b], Elisabeth Bouchaud [b], Chung-Yuen Hui [c,*]

[a] Department of Mechanical Engineering, University of Colorado Boulder, Boulder, CO 80309, USA

[b] PSL Research University, ESPCI-Paris Tech, PSL*, UMR Gulliver, EC2M, 10 rue Vanquelin, 75231, Paris Cedex 05, France

[c] Department of Mechanical and Aerospace Engineering, Field of Theoretical and Applied Mechanics, Cornell University, Ithaca, NY 14850, United States

ARTICLE INFO

Article history:
Received 11 March 2016
Received in revised form 5 May 2016
Accepted 6 May 2016
Available online 11 May 2016

Keywords:
Fracture
Large deformation
Asymptotic field
Strain hardening

ABSTRACT

In a recent work, Lefranc and Bouchaud (LB) showed that the Mode I crack opening displacement in a thin sheet of Agar gel deviates significantly from the square root profile predicted by linear elastic fracture mechanics. In this letter we re-examine this problem and show that the experimentally measured crack opening displacement is consistent with the prediction based on finite elastostatics and a hyperelastic strain hardening model.

1. Introduction

Recent interest in the mechanical properties of soft materials, especially hydrogels, has motivated several studies in the fracture behavior of these gels [1–7]. Concurrently, there is a renewed interest in the analysis of the stress and deformation fields near the tip of cracks in nonlinear elastic solids subjected to large deformation [8–10]. A summary of these efforts can be found in a recent review [11]. However, most of the previous works on gel fracture focused on measuring and/or understanding the physical mechanism of fracture toughness [2–6]. There are much fewer studies linking measurements to the prediction of continuum theory. In a recent work, Lefranc and Bouchaud [1] showed that the crack opening displacement (COD) of a Mode-I crack in a thin sheet of Agar gel deviates significantly from the square root profile predicted by linear elastic fracture mechanics (LEFM). Specifically, for slower cracks where the applied displacements are small, the crack opening displacement (COD) is found to agree well with the prediction of linear elastic fracture mechanics. However, for faster cracks which correspond to higher applied displacement, the measured COD, much larger than that for slower cracks, deviates considerably from LEFM. For the fast cracks, they observed crack tip opening profile with a wedge-like shape and speculated that this deviation is associated with nonlinear elastic behavior due to large deformation at the crack tip [1].

To bring the problem into perspective, we briefly review the experiment and results of LB [1]. Their experimental set up is shown in Fig. 1. The gel sample is enclosed in a rectangular chamber consisting of two flat glass plates with a 350 μm gap. The lateral dimensions of the gel sample are: width $w = 14$ mm and length $l = 25$ mm. Since the thickness of the gel is the same as the gap between the

* Corresponding author.
E-mail address: ch45@cornell.edu (C.-Y. Hui).

http://dx.doi.org/10.1016/j.eml.2016.05.005
2352-4316/

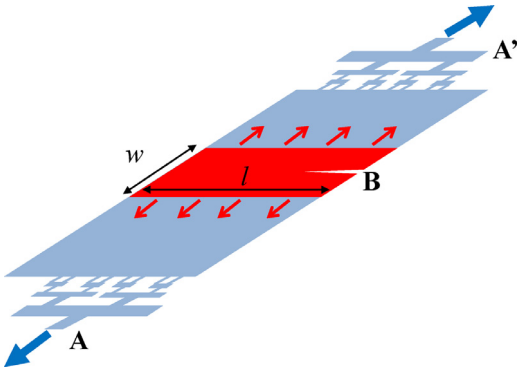

Fig. 1. Schematics of experimental set up. The gel sample is illustrated by the red rectangle. The rest of the glass chamber space on both sides of the gel sample is filled with oil which is illustrated in blue. (For interpretation of the references to colour in this figure legend, the reader is referred to the web version of this article.)
Source: Adapted from Lefranc & Bouchaud [1].

two glass plates, the surfaces of the glasses in contact with the gel are coated with an acrylamide brush to minimize adhesion and friction. The rest of chamber is filled with oil. A pre-crack of length 5 mm, labelled by B in Fig. 1, is introduced by micro-fabricating a blade pasted to the glass cell. The sample is loaded by moving the boundary between the oil/gel interface (oil is immiscible with gel) by pumping the oil out of the two ends of the chamber (A in Fig. 1) in at a constant rate Q (see Fig. 1). This procedure imposes an increasing displacement on the oil/gel interfaces (boundary between blue and red regions).

Experimentally, LB observed a regime where the crack propagates at a constant rate V which can be controlled by the pumping rate Q. Specifically, V increases from 1 μm/s to 1 cm/s as Q increases from 0.1 to 1000 μL/min. In the low velocity regime, the measured crack opening displacement (COD) behind the crack tip has the classical parabolic profile dictated by linear elastic fracture mechanics (LEFM). For an incompressible solid with Poisson's ratio being 0.5, this is

$$u_{cod} = \frac{2K_I}{3\mu}\sqrt{\frac{8d}{\pi}}, \tag{1}$$

where u_{cod} is the crack opening displacement spanning between the lower and upper crack faces, d is the distance to the deformed crack tip, and K_I is the Mode I stress intensity factor and μ the small strain shear modulus. Note that u_{cod} is twice the crack opening displacement u defined in Eq. (1) of LB [1] which is only measured from the middle plane of opened crack to the upper crack surface. In this regime, Lefranc [12] determine K_I by fitting the Williams' expansion in LEFM, including Eq. (1) as the first order term and two additional higher order terms, to the local crack opening profile measured in experiments. However, at high pumping rate (or larger applied displacements), LB discovered that the crack profile very close to the crack tip cannot be fitted satisfactorily by Eq. (1).

Here we explore the possibility that this deviation can be explained by the nonlinear straining hardening material behavior near the crack tip. Indeed, Pavan et al. [13] have observed that Agar gel exihibits strong nonlinear stress/strain behavior. For example, Lefranc [12] performed uni-axial compression test on Agar gel. The nominal compressive stress, normalized by the small strain Young's modulus $E = 3\,\mu$ (assuming incompressibility), versus nominal compressive strain is plotted in Fig. 2, which shows that deviation from linear elasticity occurs for nominal strains greater than 3%. The compressive stress–strain curve in Fig. 2 can be well fitted by an exponentially hardening incompressible material model in which the strain energy density function W has the form

$$W = \frac{\mu J_m}{2}\left[\exp\left(\frac{I_1 - 3}{J_m}\right) - 1\right], \tag{2}$$

where μ is the small strain shear modulus, I_1 is the trace of the Cauchy–Green tensor and J_m is the dimensionless strain hardening parameter. The role of J_m is to control the extensibility of the gel. A large J_m indicates small amount of strain hardening, that is, the gel is highly extensible. For example, when $(I_1 - 3)/J_m \ll 1$, the exponential strain energy density function reduces to that of the neo-Hookean or ideal rubber model which describes the entropic elasticity due to Gaussian chain statistics,

$$W = \frac{\mu J_m}{2}\left[\exp\left(\frac{I_1 - 3}{J_m}\right) - 1\right] \approx \frac{\mu}{2}(I_1 - 3) \quad (I_1 - 3)/J_m \ll 1. \tag{3}$$

By fitting the exponentially hardening model to the compression test data in Fig. 2, it is found that $\mu = 21$ kPa and $J_m = 0.1$ for the Agar gel used in the experiments of LB. To highlight the strain stiffening behavior of Agar gel, we also included in Fig. 2 the results given by the neo-Hookean model and linear elastic model with the same modulus $\mu = 21$ kPa. Clearly, the experimental data and the exponentially hardening model give higher stress than the neo-Hookean model when the compressive strain is larger than ∼5%, thus justifying the use of exponentially hardening model for Agar gel.

2. Finite element model

To simulate the deformation of the facture sample in LB's experiment, we develop a finite element model (FEM) using the commercial software ABAQUS. The gel sample is assumed to be loaded in plane stress with lateral dimensions given according to experimental geometry (25 mm × 14 mm). To simulate crack deformation, we introduce a crack of 12.5 mm in length on the left side of the sample and apply uniform normal displacements Δ on both top and bottom boundaries (see Fig. 3). The nonlinear elasticity of the Agar gel is described by the exponentially hardening model in Eq. (2) through a UHYPER subroutine in ABAQUS. The materials parameters are $\mu = 21$ kPa and $J_m = 0.1$ according to the compression test data in Fig. 2. To capture the local crack opening profile at a high spatial resolution, we take advantage of the sub-modeling approach in ABAQUS to achieve a high mesh density near the crack tip, following a similar approach described in Krishnan et al. [8]. The sub-model occupies a circular

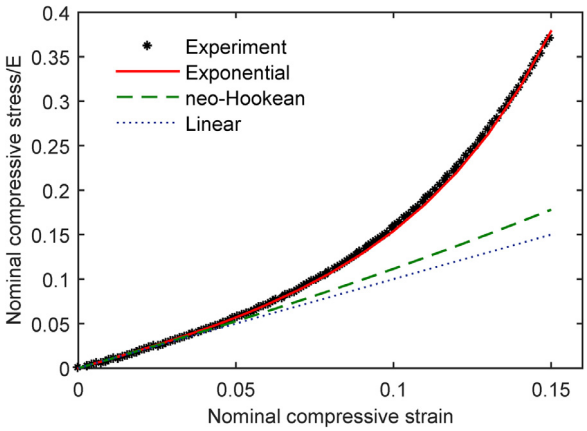

Fig. 2. Uni-axial compression data for Agar gel: the normalized compressive nominal stress is plotted as the nominal compressive strain $\lambda - 1$ where λ is the stretch ratio in the direction of compression and $E = 3\,\mu$ is the small strain Young's modulus. The experimental data (black stars) is fitted by an exponentially hardening solid given by Eq. (2) with $\mu = 21$ kPa and $J_m = 0.1$. For comparison, the results given by the neo-Hookean model and linear elastic model with $\mu = 21$ kPa are also shown.

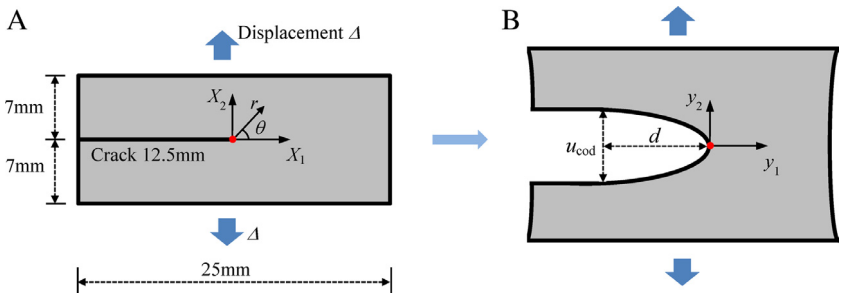

Fig. 3. Schematic of the finite element model. (A) Undeformed geometry of the model. A uniform displacement Δ is applied at the top and bottom boundary. The lateral displacement at the top and bottom boundary is constrained to be zero. (B) Deformed geometry of the crack. The crack opening displacement u_{cod} is a function of the distance d to the crack tip.

region centered at the crack tip with a radius of 250 μm. The size of this crack tip region is selected according to the local crack opening profile reported in LB [1].

There are three main differences between our FEM and the experiment reported in LB [1], which are justified below. First, unlike the experiment where the crack propagates in a steady state, in FEM we assume a static crack without propagation and focus on its deformation. The effect of crack velocity is reflected by the amount of applied displacement Δ, with the anticipation that slow cracks open less than fast cracks. As pointed out in LB [1], rheological tests revealed that the loss modulus of Agar gels is 40 times smaller than its storage modulus across a wide frequency range (0.1–100 Hz), i.e. the gel is essentially elastic. The effect of crack velocity is likely due to rate dependent fracture processes occurring at the crack tip, which can be decoupled from the deformation analysis in our FEM. Second, as noted in LB's work [1], because the displacement is imposed by moving the oil/sample interface, the stiffness of the loading system is low. As a result, the normal displacement imposed on the sample boundary is not exactly uniform. In principle the deformation field in the vicinity of the crack tip, e.g. at a length scale of 100 μm, should be insensitive to variations of the applied displacement on the boundaries which is ∼10 mm away from the crack tip, as long as these variations give the same average displacement. Therefore in the finite element model we assume a uniform applied normal displacement on the specimen boundary, and use it as an adjustable parameter to obtain the best fit to the measured crack opening profile. Further discussions on the boundary condition are provided in the Appendix. Third, in experiments the crack length varies as the crack propagates while in FEM we used a fixed crack length of 12.5 mm (see Fig. 3). To justify the crack length selected, we have also explored two additional crack lengths in our FEM, i.e. 6.25 and 18.75 mm, and found that the local crack opening displacement is insensitive to the crack length used.

3. Results

3.1. Crack opening profile

We first present the FEM results for the two cases reported in LB [1] with different crack propagation velocities: 1 cm/s and 3 μm/s. These two cases will be referred as the fast crack and slow crack hereafter.

In Fig. 4(A), we plot the local crack opening profile for the fast crack (1 cm/s), i.e. the crack opening displacement

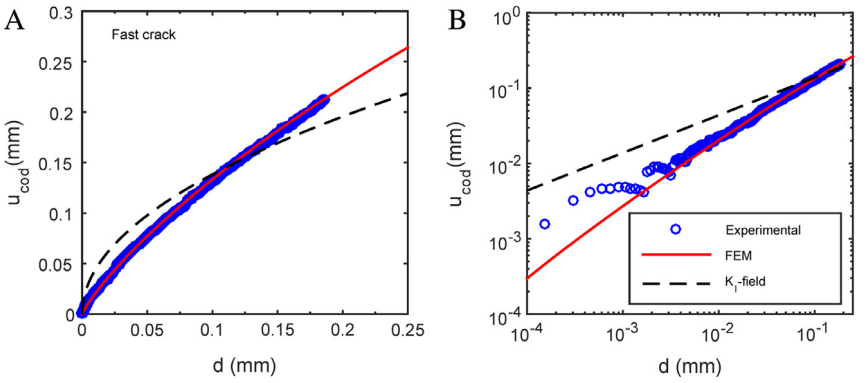

Fig. 4. Crack opening displacement for fast crack: FEM results and experiment data (a) linear scale (b) log–log scale. The symbols represent experimental data, the solid line is given by the FEM result, and the dashed line is given by Eq. (1) with $K_I = 273$ Pa m$^{1/2}$.

u_{cod} versus the distance d to the deformed crack tip. The FEM result (solid line), obtained using a normal displacement $\Delta = 0.61054$ mm, fits the experimental data (symbols) well. Also plotted is the first order K_I-field solution in Eq. (1) given by LEFM. The stress intensity factor K_I is set to be 273 Pa m$^{1/2}$ according to Lefranc [12] where K_I was determined based on the detailed crack tip deformation field measured by digital image correlation. It is clear that the FEM result gives a much better fit to the experimental data than the K_I field. Specifically, the experimental data exhibit a significantly sharper crack opening profile than the parabolic profile predicted by the K_I field. Such a sharp profile is well captured by the FEM result. This is also evident in the log–log plot of the same data shown in Fig. 4(B). The K_I field solution, which predicts $u_{cod} \sim d^{1/2}$, asymptotically deviates from the experimental data as d approaches 0. Fig. 4(B) shows oscillations in the experimental data when $d < 5$ μm. We believe this is due to experimental uncertainty at such a small length scale.

Similarly, Fig. 5(A) and (B) plot crack opening profile for the slow crack (3 μm/s) in linear and log–log scales, respectively. To fit the experimental data, we used a normal displacement $\Delta = 0.1397$ mm, much smaller than that for the fast crack. The stress intensity factor for the K_I field was also determined in Lefranc [12] which is $K_I = 84$ Pa m$^{1/2}$. In Fig. 5(A), the FEM result shows a better fit to the experimental data than the K_I field. However, it should be noted that LB demonstrated that LEFM solutions can also fit the experimental data well by including higher order terms in the Williams' expansion (up to the third order term) [1]. The log–log plot in Fig. 5(B) reveals that both the FEM result and K_I-field are asymptotically close to the experimental data as d approaches 0. This suggests that unlike the fast crack, the nonlinear effects for the slow crack is confined in a region surrounding the crack tip with a size much smaller than the experimental detection limit (i.e. ∼1 μm). This is possible since the applied displacement Δ for slow crack is only about 20% of that for the fast crack.

Long et al. [9] obtained the first-order asymptotic expansion of the crack opening displacement of a Mode I plane stress crack in an exponentially hardening solid. The one-sided crack opening displacement is:

$$y_1 = Hr\,(-J_m \ln(r/r_0))^{-1/4},$$
$$y_2 = r\sqrt{-J_m \ln(r/r_0)}, \quad r \to 0 \tag{4}$$

where H (< 0) and r_0 are parameters that cannot be determined by asymptotic analysis, y_1 and y_2 are the deformed coordinates of the crack surface (see Fig. 3B), and r is the distance from the crack tip in the undeformed configuration (along the direction $\theta = \pi$ as shown in Fig. 3A). It must be noted that the asymptotic expansion in Eq. (4) has a limited region of dominance and is valid only for very small r. Thus when fitting Eq. (4) to the FEM result, the data points closer to crack tip (with smaller r and smaller y_1 and y_2) should be assigned more weight during fitting. Ideally this can be achieved by taking a subset of the FEM data with r less than a threshold. However, this threshold, which reflects the region of validity of Eq. (4), is not known a-priori. In addition, the fact that the fitting parameter r_0 is inside the argument of the logarithmic function implies that y_2 is very insensitive to the change in r_0. As a result, the value of r_0 can be extremely sensitive to the subset of FEM data used for fitting. To provide more weight to data points closer to crack tip while avoiding artificially picking a subset of the FEM data as the input data for fitting, we performed least square fitting in log–log scale, i.e. in terms of $\ln(y_1)$, $\ln(y_2)$ and $\ln(r)$. This method is applied to the crack opening profile for the fast crack case, i.e. $\Delta = 0.61054$ mm, resulting in $r_0 = 20.8$ mm and $H = -0.86$. As shown in Fig. 6(A) and (B), the asymptotic behavior given by (4) is in good agreement with our FEM result for $r <\sim 50$ μm.

It is often convenient to express the crack opening profiles in terms of the deformed configuration, i.e. u_{cod} versus d (see Fig. 3(B)), since r, the distance to crack tip in undeformed configuration, may not be directly measureable in experiments (e.g. in the experiment of LB). To obtain an asymptotic solution for u_{cod} versus d, we first define the following normalization for y_1 and y_2:

$$\bar{y}_1 = \frac{J_m^{1/4} y_1}{r_0 |H|}, \quad \text{and} \quad \bar{y}_2 = \frac{y_2}{r_0 \sqrt{J_m}} \tag{5a}$$

where $\bar{y}_1$ and $\bar{y}_2$ are dimensionless. As shown in Long and Hui [11], the asymptotic solution in Eq. (4) leads to the following equation for the crack opening profile:

$$\bar{y}_2 \approx -\bar{y}_1 [-\ln(-\bar{y}_1)]^{1/4} \times \sqrt{-\ln\left(-\bar{y}_1 [-\ln(-\bar{y}_1)]^{1/4}\right)}. \tag{5b}$$

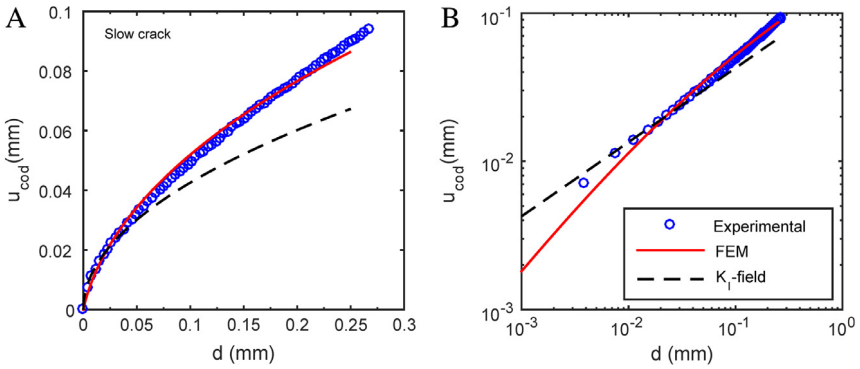

Fig. 5. Crack opening displacement for slow crack: FEM results and experiment data (a) linear scale (b) log–log scale. The symbols represent experimental data, the solid line is given by the FEM result, and the dashed line is given by Eq. (1) with $K_I = 84$ Pa m$^{1/2}$. (For interpretation of the references to colour in this figure legend, the reader is referred to the web version of this article.)

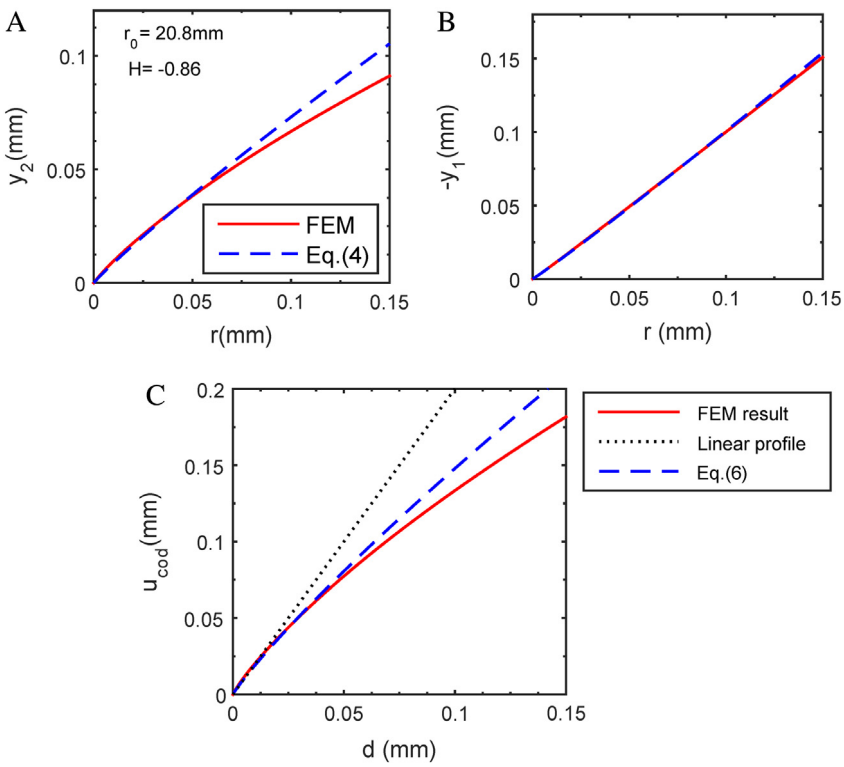

Fig. 6. Comparison between FEM result and asymptotic solution. The FEM result (solid line) is based on an applied displacement of $\Delta = 0.61054$ mm. The asymptotic solution is given by Eqs. (4) and (6) with $r_0 = 20.8$ mm and $H = -0.86$. (A) y_2 versus r, (B) $-y_1$ versus r, (C) u_{cod} versus d. The linear profile is given by $u_{cod} = 2d$ to guide the view of the initial wedge-like crack opening profile.

Since $u_{cod} = 2y_2$ and $d = -y_1$, Eq. (5b) gives the following asymptotic solution for the crack opening displacement:

$$u_{cod} \approx 2r_0\sqrt{J_m}\bar{d}\left[-\ln\left(\bar{d}\right)\right]^{1/4} \times \sqrt{-\ln\left(\bar{d}\left[-\ln\left(\bar{d}\right)\right]^{1/4}\right)}, \quad \bar{d} = \frac{J_m^{1/4} d}{r_0\,|H|}, \tag{6}$$

where $\bar{d}$ (see Eq. (6)) is the normalized distance to crack tip in deformed configuration.

A comparison of Eq. (6) and the FEM result is shown in Fig. 6(C). Also plotted in Fig. 6(C) is the linear crack opening profile with $u_{cod} \sim d$, which approximately represents the wedge-like shape at the crack tip. It can be seen that our asymptotic solution in Eq. (6) agrees better with the FEM result than the linear profile.

3.2. Crack tip stress field

Although the crack tip stress field was not directly measurable in LB [1], the first-order asymptotic solution for the crack tip stress field (Mode-I plane stress) with the exponentially hardening model was solved in Long et al. [9]. They showed that different Cauchy stress components exhibit different singularities. In particular,

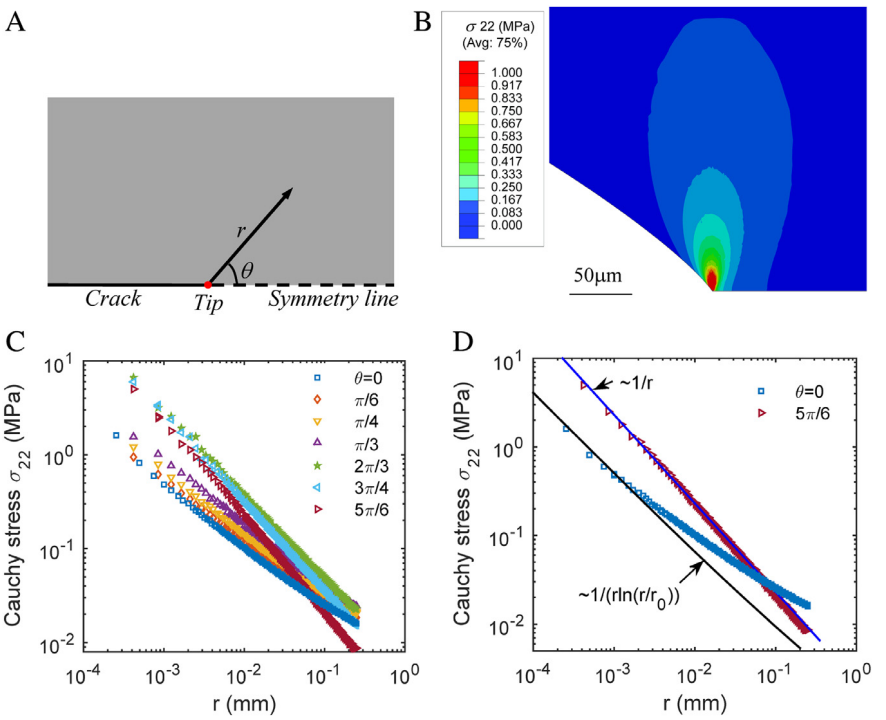

Fig. 7. Crack tip stress field for the fast crack case ($\Delta = 0.61054$ mm). (A) Undeformed geometry of the crack tip region. Polar coordinates $(r,\ \theta)$ are used to describe material points. (B) Contour plot for the Cauchy stress component σ_{22} in deformed configuration. (C) Cauchy stress σ_{22} versus undeformed radius r for different angles θ. (D) Crack tip singularity of σ_{22} along two different angles: $\theta = 0$ and $5\pi/6$, which follows $1/(r\ln(r/r_0))$ and $1/r$, respectively. Note that $r_0 = 20.8$ mm according to Fig. 6.

the normal component σ_{22} has the dominate singularity, and thus our discussion here is focused on σ_{22}. Fig. 7(A) illustrates the undeformed crack geometry to aid the discussion below, and Fig. 7(B) shows the contour plot of σ_{22} in the deformed crack tip region. Interestingly, the asymptotic solution in Long et al. [9] suggests that the singularity of σ_{22} depends on which direction the crack tip is approached (i.e. the angle θ illustrated in Fig. 7(A)):

$$\sigma_{22} \sim \frac{1}{r}, \quad \text{for } \frac{\pi}{2} < \theta < \pi \text{ or } -\pi < \theta < -\frac{\pi}{2}, \tag{7a}$$

$$\sigma_{22} \sim \frac{1}{r\ln(r/r_0)}, \quad \text{for } -\frac{\pi}{2} < \theta < \frac{\pi}{2}, \tag{7b}$$

where r_0 is the parameter introduced in Eq. (4). The first scenario above (i.e. in Eq. (7a)) is in agreement with the weakly nonlinear analysis by Bouchbinder et al. [14]. Indeed, it was argued in Long et al. [9] that for any hyperelastic model and Mode-I plane stress cracks, the Cauchy stress component σ_{22} should exhibit a $1/r$ singularity in at least an angular sector of the crack tip region so that the J-integral is path-independent. For $-\pi/2 < \theta < \pi/2$, the singularity of σ_{22} is slightly weaker than $1/r$.

Long et al. [9] showed that the stress singularities in Eqs. (7a) and (7b) are consistent with FEM results using an exponentially hardening model with $J_m = 3.5$. We include similar data in Fig. 7(C) and (D), i.e. the plot of σ_{22} versus r for different angles θ using the FEM result for the fast crack. Note in this work $J_m = 0.1$ according to experimental data of Agar gel. Fig. 7(C) shows two distinct singular behaviors for $r < 10$ μm: the cases with $\theta = 0, \pi/6, \pi/4, \pi/3$ (i.e. $<\pi/2$) follow the same singularity, and the cases $\theta = 2\pi/3,\ 3\pi/4,\ 5\pi/6$ (i.e. $>\pi/2$) follow another singularity. We take the two cases with $\theta = 5\pi/6$ and 0 as examples for further examination in Fig. 7(D). Clearly, the case with $\theta = 5\pi/6$ shows $\sim 1/r$ singularity, consistent with Eq. (7a). The case with $\theta = 0$ shows a decreasing slope in the log–log plot as r increases. Qualitatively this is consistent with Eq. (7b) which implies that

$$\frac{d[\ln(\sigma_{22})]}{d[\ln(r)]} = -1 - \frac{1}{\ln(r/r_0)}. \tag{8}$$

Since $\ln(r/r_0) < 0$, Eq. (8) shows that the absolute value of the slope of $\ln(\sigma_{22})$ versus $\ln(r)$ becomes smaller as r increases. Quantitatively Eq. (7b) captures the asymptotic behavior with $\theta = 0$ only for very small r (<5 μm). Higher order terms of the asymptotic solution are needed to obtain a better agreement with the FEM data.

4. Conclusions

Our numerical results and asymptotic analysis show that the crack opening displacement (COD) in the fracture experiments of LB can be captured using an exponentially hardening hyperelastic material model. For small applied displacements (i.e., slow crack propagation), the COD is asymptotically consistent with the K_I field predicted in LEFM. The effect of nonlinear elasticity is confined to a region very close to crack tip and not detected by

the measurements of LB [1]. However, for large applied displacements (i.e., fast crack propagation), LEFM breaks down and the exponentially hardening solid model gives much better agreement with experimental results.

Our study in this paper is based on the exponentially hardening hyperelastic model which is used to capture the severe strain stiffening effect in Agar gels (see Fig. 2). We note that a large number of biological gels, including collagen and fibrin gels exhibit strong strain stiffening behavior, as demonstrated by Storm et al. [15]. Therefore, our numerical and asymptotic solutions for crack opening profile and crack tip stresses may be used to study the fracture mechanics of a wide class of biological gels.

A question is whether it is legitimate to model the material as nonlinear elastic despite the observed rate dependence of fracture, that is, the COD increases with the crack propagation velocity. As discussed in Section 3, the Agar gel is essentially elastic based on the rheological tests reported in LB [1], suggesting that the observed rate dependence in crack propagation is due to rate dependent fracture process that can be decoupled from the stress analysis. In other words, although the Agar gel is elastic, the fracture toughness can be rate dependent. The toughness increases with crack propagation velocity, which results in a larger COD for faster cracks. Therefore, we assume no significant coupling between microscopic fracture mechanisms and continuum solutions, in the sense that the size of the fracture process zone is significantly smaller than the characteristic length scale of the continuum solution.

Finally we point out that deformation of gels can be coupled to fluid transport [16]. In particular, the high stress gradient near the crack tip can lead to significant fluid transport which in turn can affect crack opening and crack tip stress field. This effect has been studied for linear poroelastic solids [17,18] and gels [19–22]. We have neglected the effect of fluid transport by assuming a hyperelastic model for the Agar gel. Although our model is based on the rheological data in LB [1], the torsional deformation imposed in these rheological tests may not be sufficient to reveal the poroelastic behavior of the Agar gels. Here we provide further justifications. In the experiments of LB [1], the crack is propagating at steady state with a constant speed V. According to Ruina [17], the effect of fluid transport is confined in a zone surrounding the crack tip with a length scale of D/V, where D is the effective diffusivity of the solvent in the gel. To estimate the length scale D/V, we first note that $D = k\mu/\eta$, where k is the permeability of the gel, μ is the shear modulus and η is the viscosity of solvent. For the Agar gel studied in LB (1.5 wt%) [1], we estimate its permeability based on the data for Agarose gels with similar concentration, which is on the order of 100 nm^2 as reported in Johnson & Deen [23]. Using $\mu = 21$ kPa, and $\eta = 8.9 \times 10^{-4}$ Pa s for water at room temperature, the diffusivity D is found to be approximately 10^{-10} m^2/s.

For the fast crack case (see Fig. 4), $V = 1$ cm/s which means $D/V \sim 10$ nm. This length scale is much smaller than the region we study in this paper ($\sim$100 μm). Therefore, the effect of fluid transport can be neglected in our analysis of crack opening. However, for the slow crack case (see Fig. 5), $V = 3$ μm/s which means $D/V \sim 33$ μm. This estimate suggests that fluid transport may be important within $\sim$30 μm around the crack tip. In Fig. 5(B), we notice that the experimental data (symbols) starts to deviate from the FEM result (red solid line) when d is less than about 20–30 μm. Further investigations are needed to determine whether such deviation is due to the poroelastic effect.

Acknowledgments

R.L. acknowledges the start-up support from University of Colorado Boulder. E.B. acknowledges ANR (Agence Nationale pour la Recherche) for their support through the F2F and ERA projects. C.Y.H acknowledges the support of National Science Foundation, CMMI, grant no: 1537087. The authors are grateful to the anonymous reviewers for their constructive suggestions.

Appendix. Boundary conditions imposed in the FEM model

As discussed in Section 2, we assume uniform displacement on the upper and bottom boundaries of the specimen (see Fig. 2) in the FEM model, even though in the experiments of LB [1] the applied displacement at the oil–gel interface is not uniform. It is shown in Section 3 that the experimental crack opening profiles for the fast (1 cm/s) and slow cracks (3 μm/s) agree well with the FEM results using displacement $\Delta = 0.61054$ mm and 0.1397 mm, respectively. It would be interesting to compare these displacement values to experimental observations. However, LB [1] were not able to the image the oil–gel interface during crack propagation as the camera was focused at the crack tip with a field of view $\sim$300 μm that is much smaller than the sample height (14 mm).

We can obtain a rough estimate of the average displacement Δ using Qt/wh, where Q is the oil pumping rate on one side of the sample, t is the time from the beginning of experiment to the moment when the crack was imaged, $w = 25$ mm is the sample width and $h = 350$ μm is the sample thickness [1]. For the slow crack (3 μm/s), $Q = 0.1$ μL/min [12] and we assume $t = 10$–30 min. This translates $\Delta = 0.1$–0.3 mm, and the value used in our simulation ($\Delta = 0.14$ mm) falls into this range. For the fast crack (1 cm/s), it was difficult to trace the crack tip because of its high propagation speed. Instead, LB fixed the imaging field at the middle of the sample and waited for the crack to go through [12]. Based on this approach, we assume the crack tip was imaged when it has propagated for 10–15 mm (i.e. $t = 1$–1.5 s using crack speed $= 1$ cm/s). Since $Q = 10^3$ μL/min for the fast crack [12], the range of average Δ is roughly estimated to be 1.9–2.8 mm. The value used in our simulation ($\Delta = 0.61$ mm) is on the same order but smaller than this estimated range. A possible explanation is that the applied displacement at the oil–gel interface can be highly non-uniform when the crack opening is large, because of the low stiffness of the loading system (i.e. by pumping oil to drive the oil–gel interface). In this case, the part of the sample with opened crack will have much larger boundary displacement than that ahead the

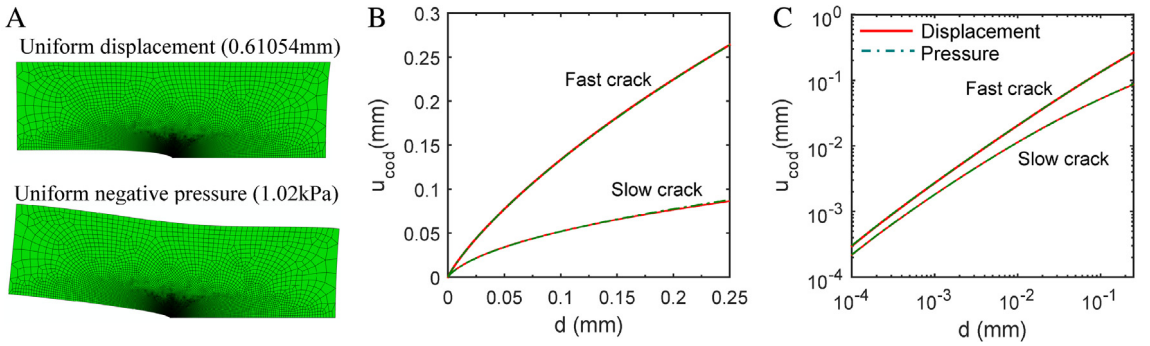

Fig. 8. Comparison of the crack opening profiles using uniform displacement or uniform negative pressure boundary conditions. (A) Global deformation with uniform displacement $\Delta = 0.61054$ mm or uniform negative pressure of 1.02 kPa. (B–C) Linear and log–log plots of the crack opening profiles in the vicinity of crack tip. The results obtained using uniform displacement $\Delta = 0.61054$ mm or 0.1397 mm are identical to those using uniform negative pressure 1.02 kPa or 197 Pa, respectively. The solid lines are results with the uniform displacement boundary condition, and the dash-dotted lines represent results with the uniform negative pressure boundary conditions.

crack tip (see Fig. 8(A)), which may lead to a higher average Δ than that needed to achieve the same crack tip field under a uniform boundary displacement.

Given the low stiffness of the loading system in LB [1], a load controlled boundary might be closer to the experimental condition. To further justify the displacement controlled boundary assumed in our simulation, we replaced the uniform displacement boundary condition (see Fig. 3) by a uniform negative pressure at the upper and lower boundaries. It was found that although the global crack deformation can be sensitive to the boundary condition, the local crack opening profiles with uniform displacement $\Delta = 0.61$ mm and 0.14 mm are identical to those with uniform negative pressure of 1.02 kPa and 197 Pa, as shown in Fig. 8. Note that the values of the negative pressure fall in the range that can be generated by the syringe pump used in the experiment.

References

[1] M. Lefranc, E. Bouchaud, Mode I fracture of a biopolymer gel: Rate-dependent dissipation and large deformations disentangled, Extreme Mech. Lett. 1 (2014) 97–103.
[2] T. Nakajima, Y. Fukuda, T. Kurokawa, T. Sakai, U.-I. Chung, J.P. Gong, Synthesis and fracture process analysis of double network hydrogels with a well-defined first network, ACS Macro Lett. 2 (2013) 518–521.
[3] M.E. Seitz, D. Martina, T. Baumberger, V.R. Kristnan, C.Y. Hui, K.R. Shull, Fracture and large strain behavior of self-assembled triblock copolymer gels, Soft Matter 5 (2009) 447–456.
[4] J.-Y. Sun, X. Zhao, W.R.K. Illeperuma, O. Chauduri, K.H. Oh, D.J. Mooney, J.J. Vlassak, Z. Suo, Highly stretchable and tough hydrogels, Nature 489 (2002) 133–136.
[5] T. Baumberger, T. Caroli, D. Martina, Solvent control of crack dynamics in a reversible hydrogel, Nature Mater. 5 (2006) 552–555.
[6] T. Nakajima, T. Kurokawa, S. Ahmed, W.-L. Wu, J.P. Gong, Characterization of internal fracture process of double network hydrogels under uniaxial elongation, Soft Matter 9 (2013) 1955–1966.
[7] K. Mayumi, J. Guo, T. Narita, C.Y. Hui, C. Creton, Fracture of dual crosslink gels with permant and transient crosslinks, Extreme Mech. Lett. 6 (2016) 52–59.
[8] V.R. Kristnan, C.Y. Hui, R. Long, Finite strain crack tip fields in soft incompressible elastic solids, Langmuir 24 (2008) 14245–14253.
[9] R. Long, V.R. Kristnan, C.Y. Hui, Finite strain analysis of crack tip fields in incompressible hyperelastic solids loaded in plane stress, J. Mech. Phys. Solids 59 (2011) 672–695.
[10] A. Livne, E. Bouchbinder, I. Svetlizky, J. Fineberg, The near-tip fields of fast cracks, Science 327 (2010) 1359–1363.
[11] R. Long, C.Y. Hui, Crack tip fields in soft elastic solids subjected to large quasi-static deformation—a review, Extreme Mech. Lett. 4 (2015) 131–155.
[12] M. Lefranc, Fracture properties of soft materials: from linear elastic fracture to damage at microscopic scale (Ph.D. dissertation), Universite Paris Sud, 2015.
[13] T.Z. Pavan, E.L. Madsen, G.R. Franck, A.A.O. Carneiro, T.J. Hall, Nonlinear elastic behavior of phantom materials for elastography, Phys. Med. Biol. 55 (2010) 2679–2692.
[14] E. Bouchbinder, A. Livne, J. Fineberg, The $1/r$ singularity in weakly nonlinear fracture mechanics, J. Mech. Phys. Solids 57 (2009) 1568–1577.
[15] C. Storm, J.J. Pastore, F.C. MacKintosh, T.C. Lubensky, P.A. Janmey, Nonlinear elasticity in biological gels, Nature 435 (2005) 191–194.
[16] W. Hong, X. Zhao, J. Zhou, Z. Suo, A theory of coupled diffusion and large deformation in polymeric gels, J. Mech. Phys. Solids 56 (2008) 1779–1793.
[17] A. Ruina, Influence of coupled deformation-diffusion effects on the retardation of hydraulic fracture (M.Sc. Thesis), Brown University, Providence, RI, 1978.
[18] C.Y. Hui, R. Long, J. Ning, Stress relaxation near the tip of a stationary Mode I crack in a poroelastic solid, J. Appl. Mech. 80 (2013) 021014.
[19] G.W. Scherer, Crack-tip stress in gels, J. Non-Cryst. Solids 144 (1992) 171–182.
[20] T. Baumberger, C. Caroli, D. Martina, Solvent control of crack dynamics in a reversible hydrogel, Nature Mater. 5 (2006) 552–555.
[21] X. Wang, W. Hong, Delayed fracture in gels, Soft Matter 8 (2012) 8171–8178.
[22] N. Bouklas, C.M. Landis, R. Huang, Effect of solvent diffusion on crack-tip fields and driving force for fracture of hydrogels, J. Appl. Mech. 82 (2015) 081007.
[23] E.M. Johnson, W.M. Deen, Hydraulic permeability of agarose gels, AIChE J. 42 (1996) 1220–1224.